

## Accepted Manuscript

### Comparison of Internal Conversion Dynamics of Azo and Azoxy Energetic Moieties through the $(S_1/S_0)_{CI}$ Conical Intersection: An Ab Initio Multiple Spawning Study

Jayanta Ghosh, Suman Bhaumik, Atanu Bhattacharya

PII: S0301-0104(18)30325-2

DOI: <https://doi.org/10.1016/j.chemphys.2018.07.041>

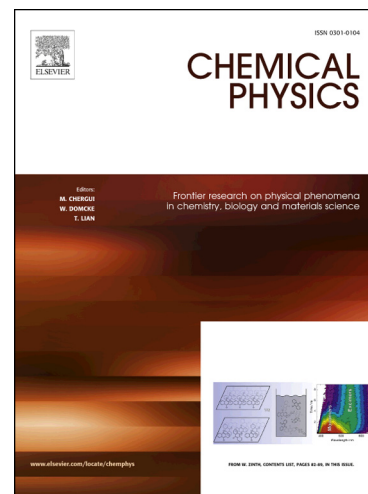
Reference: CHEMPH 10105

To appear in: *Chemical Physics*

Received Date: 5 April 2018

Revised Date: 6 July 2018

Accepted Date: 28 July 2018



Please cite this article as: J. Ghosh, S. Bhaumik, A. Bhattacharya, Comparison of Internal Conversion Dynamics of Azo and Azoxy Energetic Moieties through the  $(S_1/S_0)_{CI}$  Conical Intersection: An Ab Initio Multiple Spawning Study, *Chemical Physics* (2018), doi: <https://doi.org/10.1016/j.chemphys.2018.07.041>

This is a PDF file of an unedited manuscript that has been accepted for publication. As a service to our customers we are providing this early version of the manuscript. The manuscript will undergo copyediting, typesetting, and review of the resulting proof before it is published in its final form. Please note that during the production process errors may be discovered which could affect the content, and all legal disclaimers that apply to the journal pertain.

# Comparison of Internal Conversion Dynamics of Azo and Azoxy Energetic Moieties through the $(S_1/S_0)_{CI}$ Conical Intersection: An Ab Initio Multiple Spawning Study

Jayanta Ghosh, Suman Bhaumik and Atanu Bhattacharya\*

Department of Inorganic and Physical Chemistry, Indian Institute of Science, Bangalore 560012,  
\* [atanub@ipc.iisc.ernet.in](mailto:atanub@ipc.iisc.ernet.in), [atanubhattach@gmail.com](mailto:atanubhattach@gmail.com), Ph: 91-80-22933349

## Abstract:

We have explored the nonadiabatic chemical dynamics of trans-azomethane (AM) and azoxymethane (AOM) using ab initio multiple spawning (AIMS) simulation and CASSCF theory. A trans-to-cis isomerization around the N=N bond and a pyramidalization of the N(O)=N moiety are predicted to be involved in the internal conversion process of AM and AOM molecules, respectively. AIMS-based simulation at the CASSCF(6,4)/6-31G(d) level of theory reveals that electronically excited AM and AOM molecules undergo extremely fast (approximately in 125 femtoseconds for AM and 64 femtoseconds for AOM) relaxation to the ground state via the  $(S_1/S_0)_{CI}$  conical intersection. In addition, AIMS simulation at the CASSCF(10,8)/6-31G(d) level of theory reveals that AM molecules exhibit two relaxation pathways: major (comprising 75%) channel involves an isomerization process and minor (comprising 25%) channel features the C-N bond dissociation.

## Introduction:

Energy release process of energetic materials can be initiated with a shock/compression wave, spark, or laser ignition. About a decade ago, Bernstein argued that such events generate molecules in the excited electronic states. Details of this argument with recent literature support are given elsewhere by us.[1] Therefore, it is speculative that specific topography of the excited electronic potential energy surfaces (PESs) will determine and control the relaxation steps for the electronically excited energetic molecules. In particular, conical intersections, which arise due to the crossing of multidimensional electronic potential energy surfaces (PESs) and due to breakdown of the Born-Oppenheimer approximation, may play an important role in the initial relaxation step of energetic molecules following electronic excitation.[1-6] One of the most important consequences of the presence of conical intersections is to allow extremely fast and efficient relaxation of the electronically excited molecules from upper to the lower electronic state. This includes internal conversion (a physicochemical process by which electronically excited molecules are relaxed back to the lower electronic state of the same spin, converting electronic excitation energy to the vibrational energy on the lower potential energy surface). Therefore, understanding internal conversion process of energetic moieties through the conical intersections between the first electronically excited singlet state  $S_1$  and the ground singlet state  $S_0$  (this conical intersection is referred to as  $(S_1/S_0)_{CI}$ ) is an important pursuit if we want to understand the initial step of energy release mechanisms and dynamics of energetic molecules fundamentally.[1]

Performance of high energy density materials is often judged based on detonation pressure and velocity. Synthetic organic chemists often introduce certain (energetic) functional groups as substituents into candidate compounds to improve detonation properties of energetic molecules. For a long time, this idea has been a very effective and widely-used method for the synthesis of better energetic materials. Two very frequently-used energetic functional groups include azo and azoxy.[7-8] It has been irrevocably observed that these functional groups efficiently enhance detonation performance of the candidate molecules. Hence, one obvious question arises: what is the mechanisms and dynamics of the internal conversion process of azo and azoxy energetic functional groups? The present article is focused on this question.

In our Chemical Dynamics Lab at the Indian Institute of Science, for last few years, we have been using multi-configuration-based methodologies coupled with *ab initio* multiple spawning (AIMS) method to explore the internal conversion of electronically excited energetic molecules through the conical intersections. Our primary motivation in this effort is to explore the correlation between the nature of the internal conversion of energetic molecules (which is the initial step of the relaxation process of energetic molecules following electronic excitation) and functional group-based superior performance of energetic moieties. Continuing with this theme of research, in the present contribution, we have explored, compared and contrasted internal conversion process of trans-azomethane (AM) and azoxymethane (AOM). These two molecules contain azo ( $-N=N-$ ) and azoxy ( $-N(O)=N-$ ) energetic groups, respectively (see Figure 1 for chemical structure). We have selected these two model systems with an expectation that these two molecules would unravel salient features of the internal conversion process for azo and azoxy energetic moieties through the  $(S_1/S_0)_{CI}$  conical intersection.

## Computational Methods

We have used complete active space self-consistent field (abbreviated as CASSCF) wavefunction to perform mixed quantum-classical *ab initio* molecular dynamics (abbreviated as AIMD). In this method, the time evolution of an electronically excited system (nuclei) is modeled classically, while the energies of the relevant electronic states are computed “on the fly” using *ab initio* quantum mechanical (QM) method. In CASSCF theory, the time-independent electronic states (ground or electronically excited) are described using linear combination of Configuration State Functions (abbreviated as CSFs).[9] Each CSF features an antisymmetrized product (Slater determinant) of one electron molecular orbitals (MOs). Therefore, in the CASSCF theory, both the configuration mixing coefficients and the MO expansion coefficients are variationally optimized. For the present work, we have used state-average CASSCF (abbreviated as SA-CASSCF) electronic wavefunction to explore the nonadiabatic chemical dynamics of energetic molecules through the  $(S_1/S_0)_{CI}$  conical intersection. A SA-CASSCF wavefunction gives equal weights to several roots (several electronic states which are chemically important or nonadiabatically coupled).

We have already stated that electronic part of the total wavefunction is represented by SA-CASSCF wavefunction (which is considered to be time-independent in the present work). For the AIMD simulations, *ab initio* Multiple Spawning (abbreviated as AIMS) method,[10] which was developed by the Martinez group, is used to represent time-dependent nuclear wavefunction. The travelling frozen (with fixed width) Gaussian basis (under frozen Gaussian approximation) is used to expand the nuclear wavefunction. The centre of each Gaussian follows classical equation of motion. Details are given elsewhere.[10,11]

Each AIMS simulation starts with a single initial trajectory basis function (TBF). Typically different initial TBFs are created on the excited state surface with the help of different initial conditions. These different initial TBFs are then run independently. In all AIMS simulations, initial positions and momenta are sampled from the Wigner distribution for the ground vibrational state (under harmonic oscillator approximation) on the ground electronic state surface. Although AIMS simulation may start with a single TBF on the upper electronic state (assuming all the population on the upper excited state), unique spawning mechanism of AIMS methodology allows to spawn (generate) new TBF on the lower electronic state surface, if the strength of nonadiabatic coupling (which depends inversely on the energy difference between the coupled electronic states) increases beyond a certain threshold value (CSThresh which is taken as 3.0 a.u. in the present work). This, in turn, transfers population from upper state to the lower state stochastically. It is quite implicit that the nonadiabatic coupling is stronger near conical intersection (where potential energy surfaces cross each other, creating, in principle, degenerate point on the potential energy landscape) than that near the Franck-Condon region (where upper and lower potential energy surfaces energetically stay well-separated). Therefore, spawning occurs primarily near conical intersection region in AIMS simulation. More details of the spawning mechanisms are given in Martinez’s publications.[10,11]

In the present work, the ultrafast nonadiabatic relaxation dynamics of different energetic molecules from the first singlet ( $S_1$ ) electronically excited state to the  $S_0$  ground states is studied using AIMS module with the SA-CASSCF wavefunction and the 6-31G(d) basis set, as

implemented in Molpro.[12] The simulation time step is set to be 20 atomic unit (or 0.48 femtosecond) for regions far away from conical intersection (regions with  $CSThresh < 3.0$  a.u.) and the same changes to 5 atomic unit (or 0.12 femtosecond) for regions near the conical intersection (regions with  $CSThresh > 3.0$  a.u., indicating strong nonadiabatic coupling). Furthermore, the active space (which decides the number of the configuration state function involved) used to construct the SA-CASSCF wavefunction for the AM and AOM molecules is shown in Figure 2(a) and (b), respectively. Appropriateness of the selected active space is discussed in the Results and Discussion section.

In addition to the AIMS simulations, the  $(S_1/S_0)_{CI}$  minimum energy conical intersection (which is abbreviated as MECI), geometries for the AM and AOM molecules are also optimized with SA-CASSCF wavefunction and 6-31G(d) basis set using the algorithm implemented in Gaussian 09.[13] We shall note that this MECI geometry quite resembles spawned geometries (at these geometries 50% of the upper state population is transferred to the lower state) sampled from the AIMS simulations.

## Results and Discussion:

The most stable geometries of AM and AOM (referred to as  $S_{0,Opt}$ ), optimized at the CASSCF(6,4)/6-31G(d) level of theory, are illustrated in Figure 3. For both molecules, C-N=N-C and C-N(O)=N-C moieties exhibit planar structure (note the C1N1N2C2 and C1N1O1N2 dihedral angles given in Figure 3). Furthermore, the N=N bond distance does not change significantly upon N-oxide formation.

We have computed the vertical excitation energies of the AM and AOM molecules using the SA-CASSCF theory with different basis sets (6-31G(d), 6-31+G(d,p), 6-311++G(d,p) and aug-cc-pVDZ) as well as including dynamical correlation (CASPT2). Different results are summarized in Table I. This table directly evidences that basis set and dynamical correlation do not play significant role in the present computation. The  $S_1$  state of AM exhibits the vertical excitation energy of 3.95 eV at the SA-CASSCF(6,4)/6-31G(d) level of theory. Furthermore, a good agreement is found between the computed vertical excitation energy for the  $S_1(n,\pi^*)$  excited state of AM and the experimental value of 3.6 eV.[14] This excitation energy is also in good agreement with the computed excitation energy of the same molecule which is recently reported by Gordon and co-workers.[15] This comparison of the vertical excitation energies validates appropriateness of the (6,4) active space for the present CASSCF-computations of the AM molecules. Finally, Figure 4 depicts the orbitals involved during the electronic excitation of the AM molecule. The CSF associated with the highest coefficient shows that the  $S_1$  excited state of AM is of  $(n,\pi^*)$  character. Both nonbonding and  $\pi^*$  orbitals are localized in azo (N=N) group only.

Similar to the AM results, Table I also suggests that both basis set and dynamical correlation do not play important role for the AOM molecule. The vertical excitation energy associated with the  $S_1$  excited state of AOM is computed to be 4.71 eV at the SA-CASSCF(6,4)/6-31G(d) level of theory. At all levels of theory (with different basis sets and including dynamical correlation), we find that AOM exhibits higher (more than 0.5 eV) vertical

excitation energy for the  $S_1$  excited state as compared to that of the AM molecule. In addition, as shown in Figure 4, the  $S_1$  excited state of AOM exhibits an ( $n,\pi^*$ ) electronic excitation character; however, in contrary to the AM molecule, the nonbonding orbital in AOM is not localized on the  $N=N$  moiety. Rather, it is found to be localized at the O-end of the azoxy moiety. We argue that this causes slightly higher vertical  $S_1$  excitation energy for the AOM molecule than the AM molecule.

To the best of our knowledge, thus far, no literature is reported on the experimental vertical excitation energy for the  $S_1(n,\pi^*)$  excited state of the AOM molecule. This is why it is impossible to validate the (6,4) active space for the AOM molecule by comparing theoretical results with the experimental ones. For the AOM molecule, however, we argue that observation of very similar vertical excitation energies computed at all levels of theory (CASSCF and CASPT2 with different basis sets) with the (6,4) active space validates appropriateness of this active space for the present CASSCF-computation of the AOM molecules.

As, in the present work, we are only interested in internal conversion of AM and AOM molecules through the respective  $(S_1/S_0)_{CI}$  conical intersection, we directly turn our attention to the optimized geometry of the respective  $(S_1/S_0)_{CI}$  MECI. The optimized geometries of the  $(S_1/S_0)_{CI}$  both for the AM and AOM molecules are depicted in Figure 3. The  $(S_1/S_0)_{CI}$  geometry of AM exhibits significantly different  $C1N1N2C2$  dihedral angle as compared to its  $S_{0,Opt}$  geometry: the  $C1N1N2C2$  dihedral angle is found to be  $\sim 94^\circ$  at the optimized conical intersection geometry; whereas the same is found to be  $\sim 180^\circ$  at the FC-point (ground state equilibrium geometry) of the  $S_1$  surface. Geometrical transformation from the  $S_{0,Opt}$  to the  $(S_1/S_0)_{CI}$  suggests that the AM molecule attempts to undergo trans-to-cis isomerization while evolving from the FC point of the  $S_1$  surface to the  $(S_1/S_0)_{CI}$ . Similar trans-to-cis isomerization has also been predicted for the same molecule recently by Gordon and co-workers.[15]

On the contrary, the  $(S_1/S_0)_{CI}$  geometry of AOM does not predict any trans-to-cis isomerization. Instead, the  $-N(O)=N-$  moiety is found to lose planarity of the moiety at the  $(S_1/S_0)_{CI}$  conical intersection (see Figure 3). The  $C1N1O1N2$  dihedral angle is found to be  $\sim 119^\circ$  at the optimized conical intersection geometry; whereas, the same is found to be  $\sim 180^\circ$  at the FC-point (ground state equilibrium geometry) of the  $S_1$  surface. More details of this geometrical transformation will be evident soon when we shall discuss AIMS results.

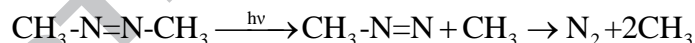
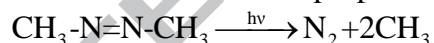
We have performed all AIMS simulations which assume entire population on the  $S_1$  excited state. Total 28 and 36 initial conditions are selected for the AM and AOM molecules, respectively at the CASSCF(6,4)/6-31G(d) level of theory. These initial conditions are randomly sampled from the ground state vibrational Wigner distribution calculated under the harmonic oscillator approximation. The scheme is already implemented in AIMS-Molpro module. Figures 5(a) and (b) depict the change of average population of the AM and AOM molecules, respectively, on the respective  $S_0$  ground and the  $S_1$  excited states as a function of the simulation time (expressed in femtoseconds). We find that the quenching of the  $S_1$  excited state population to the ground electronic state for both molecules is extraordinarily fast (occurs in approximately 125 femtoseconds for AM and in approximately 64 femtoseconds for AOM). Our AIMS-predicted internal conversion time scale of AM is in very good agreement with the recent surface-hopping results which predict 200 fs for the same.[28]



Figures 5(a) and (b) also depict snapshots of geometries sampled at two different simulation times: one at zero femtosecond and another at the simulation time when 50% excited state population is quenched. Geometries sampled at zero femtosecond (from Wigner distribution) closely resemble the ground state optimized geometry of the respective molecule. On the other hand, geometries sampled at the simulation time when 50% excited state population is quenched back to the ground state closely resemble the minimum energy ( $S_1/S_0$ )<sub>CI</sub> conical intersection geometry (as depicted in Figure 3 for the respective molecule). Furthermore, AIMS simulation also reveals that a trans-to-cis isomerization mechanism is involved in the internal conversion process of the AM molecule; however, a pyramidalization of the  $-N(O)=N-$  azoxy moiety is involved in the internal conversion process of the AOM molecule. These different structural evolutions become clearly evident when we inspect the variation of the average C1N1N2C2 dihedral angle of the AM molecule and the average C1N1N2O1 dihedral angle of the AOM molecule as a function of simulation time (see Figure 6(a) and (b), respectively).

At the SA-CASSCF(6,4)/6-31G(d) level of theory, we have also monitored possible C-N bond cleavage of the AM and AOM molecules (and N-O bond cleavage of the AOM molecule) during the internal conversion through the respective ( $S_1/S_0$ )<sub>CI</sub> conical intersection. Figure 7(a) shows no significant elongation of the C-N bond length during the relaxation process of the AM molecule from the  $S_1$  excited state to the  $S_0$  excited state. Similar observation is also evident in Figure 7(b) for the AOM molecule. In addition, Figure 7(b) also exhibits that the N-O bond does not undergo significant elongation during the internal conversion process of the AOM molecule.

Photophysics and photochemistry of the AM [17-30] molecule have attracted interest of scientific community for a long time. Several reports support that the AM molecule, following photoexcitation to the low-lying electronically excited states, undergoes C-N bond dissociation. Following photodissociation mechanisms are proposed:



Here, first and second mechanisms exhibit concerted and step-wise processes, respectively. However, on the contrary, our present study performed at the SA-CASSCF(6,4)/6-31G(d) level of theory reveals only non-dissociative internal conversion route for the AM molecule. In order to uplift this disagreement, we have made an attempt to explore the internal conversion process of the AM molecule at the SA-CASSCF(10,8)/6-31G(d) level of theory.

The orbitals optimized for the (10,8) active space is shown in Figure 2(c) which features that this active space includes several antibonding  $\sigma^*$  orbitals (including the C-N antibonding orbital  $\sigma_{\text{CN}}^*$ ). AIMS simulation results with the (10,8) active space are summarized in Figures 8(a), (b) and (c). Quite interestingly, at the SA-CASSCF(10,8)/6-31G(d) level of theory, two relaxation channels for the AM molecule are identified: one leads to the trans-to-cis isomerization and other renders the C-N bond dissociation. AIMS simulation results at the CASSCF(10,8)/6-31G(d) level of theory, which are averaged over 60 samples, further reveal the branching ratio of isomerization and dissociation as 3 : 1. Therefore, majority (75%) of the trajectories represent the trans-to-cis isomerization and the C-N bond dissociation represents a minor channel in ultrafast relaxation of the AM molecules from the  $S_1$  excited state to the ground state.

Figures 8(a) and (b) depict the ground and excited state average populations as a function of simulation time (in femtoseconds), exhibiting the isomerization and C-N bond dissociation channels, respectively. The excited state lifetimes (defined by 50% population decay time) are identified to be 126 fs along isomerization channel and 129 fs along the C-N bond dissociation channel. Exact nature of these channels is confirmed by inspecting time-evolution of the structural parameters (associated with all trajectory basis functions) of the AM molecule during simulation. For brevity, here, we present the change of the average C-N bond length as a function of the simulation time for trajectories representing only C-N bond dissociation. Trajectories associated with the isomerization process do not exhibit substantial C-N bond elongation (similar to Figure 7(a)).

Zewail and co-workers, through the femtosecond time-resolved mass spectrometry experiment, [17,27] observed that electronically excited AM decays in 70 fs and the  $\text{CH}_3\text{N}_2$  fragment is generated also in 70 fs after the photoexcitation of the AM molecule. Furthermore, Zewail and co-workers concluded that the first C-N bond dissociation of the AM molecule occurs only on the ground state following internal conversion through the isomerization process. Recent surface-hopping study, in concordance with Zewail and co-workers' findings, also predicts that AM molecules relax back to the ground-state minima before the first CN dissociation takes place.[28] In this context, present AIMS simulation finds slightly different explanation for Zewail and co-workers' experimental findings. In concordance with Zewail and co-workers' observations, AIMS simulation predicts similar time scale for the decay of the parent AM molecules through isomerization and the first C-N bond dissociation pathway. However, AIMS simulation predicts that C-N bond dissociation is not initiated only after the internal conversion of the AM molecules to the ground state through isomerization process. The C-N bond dissociation is, in fact, a minor channel of relaxation of AM molecule from the  $S_1$  excited state.

## General Discussion and Conclusions:

In general, the internal conversion processes are found to mediate via the conical intersections (CI are also called photochemical funnels). Near the CI, a strong coupling between electronic states completely breaks down the Born-Oppenheimer adiabatic approximation and the dominant term that controls the internal conversion processes near the CI region is the nonadiabatic coupling term. During the internal conversion process, geometry associated with a conical intersection is often found to be related to the expected outcome. Therefore, characterization of chemically relevant minimum energy conical intersection (MECI) serves as an important component in the development of theoretical understanding of the internal conversion process of molecules following electronic excitation.

For polyatomic molecules, two adiabatic electronic states, even with the same symmetry, may intersect and form a conical intersection. Only for diatomic molecules, where there is only one degree of freedom, electronic states with same symmetry do not cross, yielding a non-crossing rule. At a conical intersection, one can distinguish two directions,  $\vec{g}$  and  $\vec{h}$  such that if one were to plot the energy in the subspace of these two geometric variables (combination of bond lengths, angles, etc.), the potential energy would have the form of a double cone in the



region of the degeneracy. The  $g-h$  internal coordinates lift the degeneracy linearly near conical intersection. Therefore,  $g-h$  plane explores the local topography of the potential energy surface near the conical intersection.

The  $g-h$  planes near the CASSCF-optimized  $(S_1/S_0)_{CI}$  MECI of AM and AOM are shown in Figure 9. Respective vectors are also shown in the same figure. The  $\vec{g}$  vector represents the nuclear gradient of the difference between the energy of the  $S_1(n,\pi^*)$  excited state and the energy of the ground state. The  $\vec{h}$  vector is, on the other hand, represents the nonadiabatic coupling matrix element (NACME) between the ground state and  $S_1(n,\pi^*)$  excited state. Simple visual inspection reveals that the  $(S_1/S_0)_{CI}$  conical intersection of AM is a peaked type conical intersection, which leads to the prediction that the internal conversion from the  $S_1(n,\pi^*)$  excited state to the ground state should be very fast once a nonadiabatic dynamics simulation approaches this conical intersection geometry. Simple visual inspection, however, does not allow us to determine whether the  $(S_1/S_0)_{CI}$  of AOM is peak or slope type. Nonetheless, Figure 9 shows that the branching plane gets affected by N-oxide formation of the azo group and the consequence is evident in faster internal conversion dynamics predicted for AOM as compared to AM. Here we note that the nature of the local topography (whether peak or slope type) can be determined mathematically by calculating the projection of the state gradients along the  $\vec{g}$  and  $\vec{h}$  coordinates, as proposed by Yarkoni, Bearpark, Atchity and Others.[31] In the present work, we have not performed such mathematical analysis.

Internal conversion dynamics of the AM molecule from the  $S_1(n\pi^*)$  electronically excited state to the ground electronic state has attracted immense attention for a long time because this molecule undergoes dissociation (which yields  $N_2$  and  $CH_3$  products) on the ground potential energy surface immediately following the internal conversion.[17-30] Furthermore, dissociation mechanism of this molecule has raised several controversial questions, including involvement of concerted or step-wise process. The timescale for the internal conversion from the  $S_1(n\pi^*)$  excited state to the ground  $S_0$  state of AM was experimentally observed to be  $70 \pm 10$  fs.[17] The same is predicted to be 125 fs from our present AIMS simulation at the SA-CASSCF(6,4)/6-31G(d) level of theory. This is why we believe that our AIMS-predicted internal conversion time scale is in close agreement with that observed experimentally. Furthermore, our AIMS-predicted internal conversion time scale is better agreement with the experimental result than recent surface-hopping results which predict 200 fs for the same.[28]

The AIMS-simulated lifetime of the  $S_1(n,\pi^*)$  excited state of AM and AOM is found to be  $\sim 125$  and 64 femtoseconds, respectively. No evidence is found for elimination of  $CH_3$  (for both molecules or O elimination for azoxy molecule) on the excited state surface at the CASSCF(6,4)/6-31G(d) level of theory. A trans-to-cis isomerization is observed for the azo group and an out-of-plane bending of the  $-N(O)=N-$  group (leading to pyramidalization of this moiety) is observed for the azoxy group during the internal conversion process.

Photoinduced trans-to-cis isomerization about C=C bond represents one of the well-studied mechanisms for converting light energy into mechanical motion on a molecular scale.[32] Similar trans-to-cis photoinduced isomerization is exhibited by N=N bond; however,

upon N-oxide formation, this photophysical mechanism is changed to pyramidalization of the N(O)=N moiety. Thus, in this present work, for the first time, we used *ab initio* multiple spawning (AIMS) methodology with complete active space self-consistent field theory to compare and contrast similarities and differences of the internal conversion process of azo and azoxy energetic groups.

Finally, in the present work, we have found an alternative explanation for the dissociation mechanism of AM molecules following electronic excitation. Previous mass spectrometric experimental study [17,27] and surface hopping theoretical [28] study support that AM molecules relaxes back to the ground state before the first C-N bond breaks. However, present AIMS simulation at the CASSCF(10,8)/6-31G(d) level of theory reveals that the C-N bond dissociation is a minor channel (comprising 25% of all trajectories) in the overall relaxation process of AM molecules from the  $S_1$  excited state.

## Acknowledgements

We thank Prof. Todd Martinez (Stanford University) for helping us understand different aspects of AIMS theory and its interpretation in Molpro. We thank Dr. Sai G. Ramesh for selflessly maintaining departmental computational cluster facility. All computations were performed in this computational cluster facility.

## References:

1. J. Ghosh, H. Gajapathy, A. Konar, G. M. Narasimhaiah, and A. Bhattacharya, *Sub-500 fs electronically nonadiabatic chemical dynamics of energetic molecules from the  $S_1$  excited state: Ab initio multiple spawning study*, J. Chem. Phys. 147 (2017) 204302.
2. A. Bera, J. Ghosh and A. Bhattacharya, *Ab Initio Multiple Spawning Dynamics Study of Dimethylnitramine and Dimethylnitramine-Fe Complex to Model Their Ultrafast Nonadiabatic Chemistry* J. Chem. Phys., 147 (2017) 044308.
3. J. Ghosh, A. Bera and A. Bhattacharya, “*AIMS Simulation Study of Ultrafast Electronically Nonadiabatic Chemistry of Methyl Azide and UV-VIS Spectroscopic Study of Azido-Based Energetic Plasticizer Bis(1,3-diazidoprop-2-yl)malonate*” Chem. Phys., 494 (2017) 78.
4. J. Ghosh and A. Bhattacharya, “*Prediction of Electronically Nonadiabatic Decomposition Mechanisms of Isolated Gas Phase Nitrogen-Rich Energetic Salt: Guanidium-Triazolate*” Chem. Phys., 464 (2016) 26-39.
5. A. Bera, S. Maroo and A. Bhattacharya, “*Electronically Nonadiabatic Decomposition Mechanisms of Clusters of Zinc and Dimethylnitramine*” Chem. Phys., 446 (2015) 47-56.
6. A. Bhattacharya, Y. Guo, and E. R. Bernstein, *Nonadiabatic Reaction of Energetic Molecules*

*Acc. Chem. Res.*, 43 (2010) 1476–1485.

7. D. E. Chavez, M. A. Hiskey, and D. L. Naud, *Tetrazine Explosives, Propellants, Explos., Pyrotech.* 29 (2004) 209.

8 T. M. Klapotke, *New Nitrogen-Rich High Explosives*, in Book High Energy Density Materials, Ed. T. M. Klapotke Springer, 2007, page 85-121.

[9] L. Piela, *Ideas of Quantum Chemistry*, Elsevier, 2007.

10. M. Ben-Nun, T. J. Martínez, “Ab Initio Quantum Molecular Dynamics,” *Adv. Chem. Phys.* 121 (2002) 439.

11. B. G. Levine, J. D. Coe, A. M. Virshup and T. J. Martinez, “Implementation of *ab initio* multiple spawning in the Molpro quantum chemistry package,” *Chem. Phys.* 347 (2008) 3.

12. H.-J. Werner, P. J. Knowles, G. Knizia, F. R. Manby, M. Schütz, P. Celani, Korona, T.; Lindh, R.; Mitrushenkov, A.; Rauhut, G.; Shamasundar, K. R.; Adler, T. B.; Amos, R. D.; Bernhardsson, A.; Berning, A.; Cooper, D. L.; Deegan, M. J. O.; Dobbyn, A. J.; Eckert, F.; Goll, E.; Hampel, C.; Hesselmann, A.; Hetzer, G.; Hrenar, T.; Jansen, G.; Köppl, C.; Liu, Y.; Lloyd, A. W.; Mata, R. A.; May, A. J.; McNicholas, S. J.; Meyer, W.; Mura, M. E.; Nicklass, A.; O'Neill, D. P.; Palmieri, P.; Peng, D.; Pflüger, K.; Pitzer, R.; Reiher, M.; Shiozaki, T.; Stoll, H.; Stone, A. J.; Tarroni, R.; Thorsteinsson, T.; Wang, M. MOLPRO, version 2012.1.

13. M. J. Frisch, G. W. Trucks, H. B. Schlegel, G. E. Scuseria, M. A. Robb, J. R. Cheeseman, Scalmani, G.; Barone, V.; Mennucci, B.; Petersson, G. A.; Nakatsuji, H.; Caricato, M.; Li, X.; Hratchian, H. P.; Izmaylov, A. F.; Bloino, J.; Zheng, G.; Sonnenberg, J. L.; Hada, M.; Ehara, M.; Toyota, K.; Fukuda, R.; Hasegawa, J.; Ishida, M.; Nakajima, T.; Honda, Y.; Kitao, O.; Nakai, H.; Vreven, T.; Montgomery, Jr., J. A.; Peralta, J. E.; Ogliaro, F.; Bearpark, M.; Heyd, J. J.; Brothers, E.; Kudin, K. N.; Staroverov, V. N.; Kobayashi, R.; Normand, J.; Raghavachari, K.; Rendell, A.; Burant, J. C.; Iyengar, S. S.; Tomasi, J.; Cossi, M.; Rega, N.; Millam, N. J.; Klene, M.; Knox, J. E.; Cross, J. B.; Bakken, V.; Adamo, C.; Jaramillo, J.; Gomperts, R.; Stratmann, R. E.; Yazyev, O.; Austin, A. J.; Cammi, R.; Pomelli, C.; Ochterski, J. W.; Martin, R. L.; Morokuma, K.; Zakrzewski, V. G.; Voth, G. A.; Salvador, P.; Dannenberg, J. J.; Dapprich, S.; Daniels, A. D.; Farkas, Ö.; Foresman, J. B.; Ortiz, J. V.; Cioslowski, J.; Fox, D. J. *Gaussian 09*, Revision A.1; Gaussian, Inc., Wallingford CT, 2009.

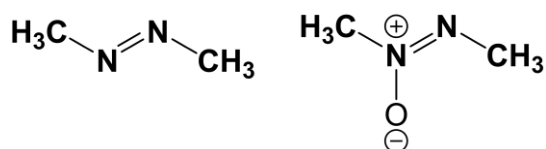
14. (a) S. S. Collier, D. H. Slater, and J. G. Calvert, “THE PHOTOCHEMISTRY OF THE AZOALKANES”, *Photochem. Photobiol.* 7 (1968) 737; (b) M. B. Robin, B. R. Hart, and N. A. Kuebler, “Electronic States of the Azoalkanes”, *J. Am. Chem. Soc.* 89 (1967) 1564; (c) P. S. Engel, *Mechanism of the Thermal and Photochemical Decomposition of Azoalkanes*. *Chem. Rev.* 80 (1980) 99–150.

15. A. Gaenko, A. DeFusco, S. A. Varganov, T. J. Martínez, and M. S. Gordon, *Interfacing the Ab Initio Multiple Spawning Method with Electronic Structure Methods in GAMESS: Photodecay of trans-Azomethane*, *J. Phys. Chem. A* **118** (2014) 10902–10908.
16. B. G. GOWENLO, AZOXYCOMPOUNDS I. THE PHOTOLYSIS OF AZOXYMETHANE, *Can. J. Chem.* **1964**, *42*, 1936.
17. E. W.-G. Diau, O. K. Abou-Zied, A. A. Scala, and A. H. Zewail, Femtosecond Dynamics of Transition States and the Concept of Concertedness: Nitrogen Extrusion of Azomethane Reactions, *J. Am. Chem. Soc.* **1998**, *120*, 3245–3246.
18. Andrew, B. K.; Burton, K. A.; Weisman, R. B. Dynamics of the two-step photodissociation of azomethane *J. Chem. Phys.* **1992**, *96*, 1111.
19. North, S. W.; Longfellow, C. A.; Lee, Y. T. The near ultraviolet photodissociation dynamics of azomethane, *J. Chem. Phys.* **1993**, *99*, 4423.
20. Fairbrother, D. H.; Dickens, K. A.; Stair, P. C.; Weitz, E. Energy content of methyl radicals produced in the UV photodissociation of azomethane, *Chem. Phys. Lett.* **1995**, *246*, 513.
21. Baggott, J. E.; Brouard, M. A.; Coles, A. Davis; Light-foot, P. D.; Macpherson, M. T.; Pilling, M. J. Product Yields and Mechanism of the Excimer Laser Photolysis of Azomethane at 193 nm *J. Phys. Chem.* **1987**, *91*, 317.
22. Geio, T.; Felder, P.; Huber, J. R. The concerted photodissociation of azomethane at 193 nm *Chem. Phys.* **1995**, *195*, 423.
23. Camp, R. N.; Epstein, I. R.; Steel, C. Theoretical Studies of the Photochemistry of Acyclic Azoalkanes *J. Am. Chem. Soc.* **1977**, *99*, 2453.
24. Hu, C.-H.; Schaefer, H. F. III The Mechanism of the Thermal Decomposition and the (n- $\pi^*$ ) Excited States of Azomethane *J. Phys. Chem.* **1995**, *99*, 7507.
25. Liu, R.; Cui, Q.; Dunn, K. M.; Morokuma, K. *Ab initio* molecular orbital study of the mechanism of photodissociation of *trans*-azomethane *J. Chem. Phys.* **1996**, *105*, 2333.
26. Cattaneo, P.; Persico, M. *Ab initio* determination of quasi-diabatic states for multiple reaction pathways *Chem. Phys.* **1997**, *214*, 49.
27. Eric W.-G. Diau and Ahmed H. Zewail, “Femtochemistry of *trans*-Azomethane: A Combined Experimental and Theoretical Study”, *ChemPhysChem* **4** (2003) 445–456.
28. B. Sellner, M. Ruckebauer, I. Stambolic, M. Barbatti, A. J. A. Aquino, and H. Lischka, “Photodynamics of Azomethane: A Nonadiabatic Surface-Hopping Study”, *J. Phys. Chem. A* **114** (2010) 8778–8785.
29. P. Cattaneo and M. Persico, “Semiclassical Simulations of Azomethane Photochemistry in the Gas Phase and in Solution” *J. Am. Chem. Soc.* **123** (2001) 7638–7645.
30. P. G. Szalay, A. J. A. Aquino, M. Barbatti and H. Lischka, “Theoretical study of the excitation spectrum of azomethane” *Chemical Physics* **380** (2011) 9–16.
31. (a) Yarkony, "Conical intersections: their description and consequences" in: *Conical Intersections*. Adv. Series in Physical Chemistry Vol. 15, edited by Domcke, Yarkony, Köppel, World Scientific 2004; (b) G. J. Atchity, S. S. Xantheas, and K. Ruedenberg, Potential energy surfaces near intersections *J. Chem. Phys.* **1991**, *95*, 1862; (c) Fabrizio Sicilia, Michael J. Bearpark, Lluís Blancafort, Michael A. Robb, *Theo. Chem. Acc.* **2007**, *118*, 241.
32. B. G. Levine and T. J. Martinez, *Isomerization Through Conical Intersections*, *Annu. Rev. Phys. Chem.* **58** (2007) 613–634.

Table I: Vertical excitation energies and energies associated with the minimum energy  $(S_1/S_0)_{CI}$  conical intersection (MECI) of trans-azomethane (AM) and azoxymethane (AOM), as computed at the CASSCF(6,4)/6-31G(d), CASSCF(6,4)/6-31+G(d,p), CASSCF(6,4)/6-311++G(d,p), CASSCF(6,4)/aug-cc-pVDZ, and CASPT2(6,4)/6-31G(d) levels of theory. Relative energies (in eV) are calculated with respect to the  $S_0$  FC point of the respective molecule.

Molecule	FC point or $(S_1/S_0)_{CI}$ MECI	Relative Energy (eV) with respect to the $S_0$ minimum				
		CASSCF(6,4)/ 6-31G(d)	CASSCF(6,4)/ 6-31+G(d,p)	CASSCF(6,4)/ 6-311++G(d,p)	CASSCF(6,4)/ aug-cc-pVDZ	CASPT2(6,4)/ 6-31G(d)
AM	$S_{1,FC}$	3.95	3.99	3.98	4.02	3.39
	$(S_1/S_0)_{CI}$	3.10	3.15	3.13	3.16	2.90
AOM	$S_{1,FC}$	4.71	4.74	4.74	4.78	4.82
	$(S_1/S_0)_{CI}$	3.38	3.39	3.46	3.74	3.72

Figure 1: Chemical Structure of *trans*-azomethane (AM, left figure) and azoxymethane (AOM, right figure).

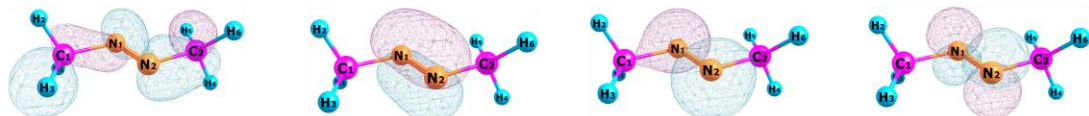


ACCEPTED MANUSCRIPT

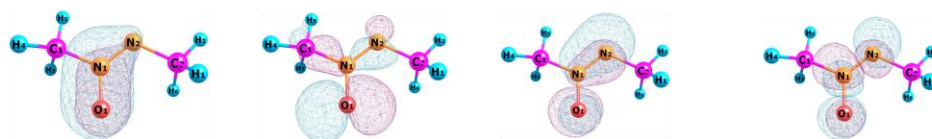


Figure 2: Orbitals used in the (6,4) active space of (a) AM and (b) AOM for the SA-CASSCF/6-31G(d) computations. (c) Orbitals used in the (10,8) active space of AM for the SA-CASSCF/6-31G(d) computations. These orbitals were obtained after optimizing the ground state geometry at the same SA-CASSCF/6-31G(d) level of theory.

(a) Active space of trans-Azomethane: @ CASSCF(6,4)/6-31G(d)



(b) Active space of Azoxymethane : @ CASSCF(6,4)/6-31G(d)



(c) Active space of trans-Azomethane: @ CASSCF(10,8)/6-31G(d)

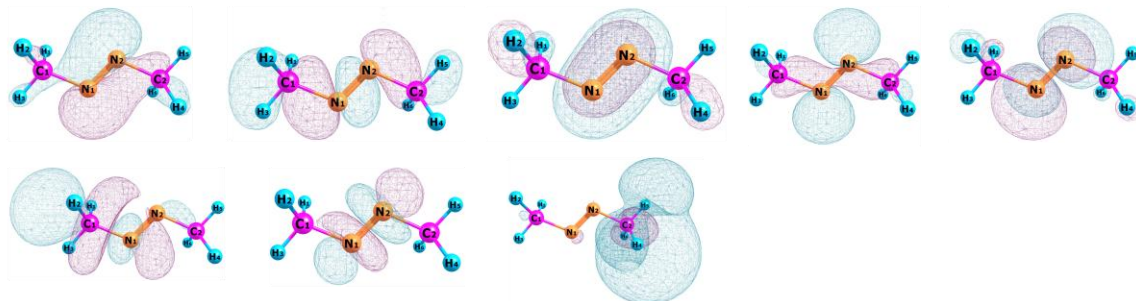


Figure 3: Optimized geometries of AM and AOM at different critical points (ground state equilibrium geometry ( $S_{0,Opt}$ ) and the  $(S_1/S_0)_{CI}$  conical intersection geometry), obtained at the CASSCF(6,4)/6-31G(d) level of theory. Bond distances are given in Å. Bond angles and dihedral angles are given in degree.

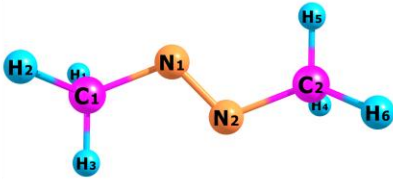
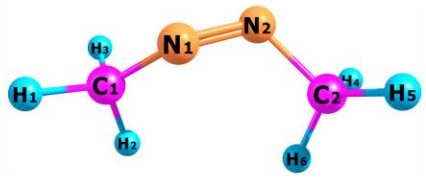
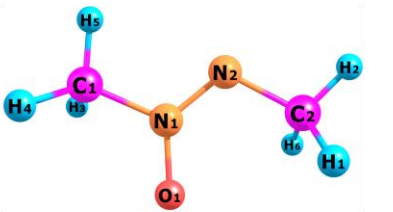
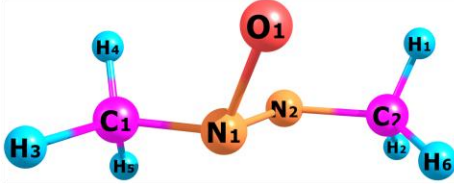
Molecules	$S_{0,Opt}$	$(S_1/S_0)_{CI}$
trans-Azomethane (AM)	 <p>C1-N1= 1.455, N1-N2= 1.237 N2-C2= 1.456, C1-N1-N2= 113.13, N1-N2-C2= 113.10, C1-N1-N2-C2= 179.93</p>	 <p>C1-N1= 1.433, N1-N2= 1.278 N2-C2= 1.462, C1-N1-N2=130.922, N1-N2-C2= 114.79, C1-N1-N2-C2= 94.172</p>
Azoxymethane (AOM)	 <p>C1-N1= 1.465, N1-N2= 1.256, N1-O1= 1.231, N2-C2= 1.449, C1-N1-N2= 117.02, N1-N2-C2= 112.90, C1-N1-O1= 116.42, C1-N1-N2-C2= 180.00, C1-N1-O1-N2= 179.99</p>	 <p>C1-N1= 1.452, N1-N2= 1.335, N1-O1= 1.419, N2-C2= 1.456, C1-N1-N2= 114.16, N1-N2-C2= 114.35, C1-N1-O1= 112.57, C1-N1-N2-C2= 178.63, C1-N1-O1-N2= 118.68</p>

Figure 4: Orbitals involved during the electronic excitation from the  $S_{0,FC}$  to the  $S_{1,FC}$  of AM and AOM, as computed at the SA-CASSCF(6,4)/6-31G(d) level of theory. These orbitals are identified from the configuration state function (CSF) with highest coefficient (value of the respective coefficient is also given).

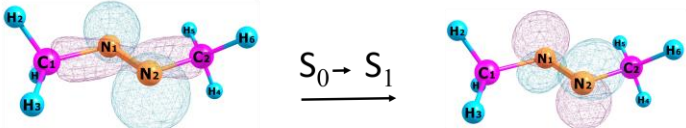
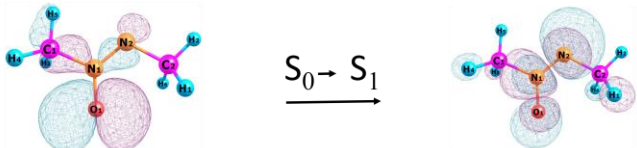
Molecule	CSF Contribution	Excitation
trans-Azomethane (AM)	0.967	
Azoxymethane (AOM)	0.963	

Figure 5: Plots of average population of the  $S_1$  excited state ( $S_1$ , blue) and the  $S_0$  ground state ( $S_0$ , red) as a function of simulation time for (a) AM and (b) AOM, as revealed by the AIMS simulation using the SA-CASSCF(6,4)/6-31G(d) wave function. Minimum energy  $(S_1/S_0)_{CI}$  conical intersection (optimized at the same level of theory) is also shown to compare with the superimposed spawning geometries. All plots represent an average of 28 independent AIMS simulations (with different initial conditions) for AM and 36 independent AIMS simulations (with different initial conditions) for AOM.

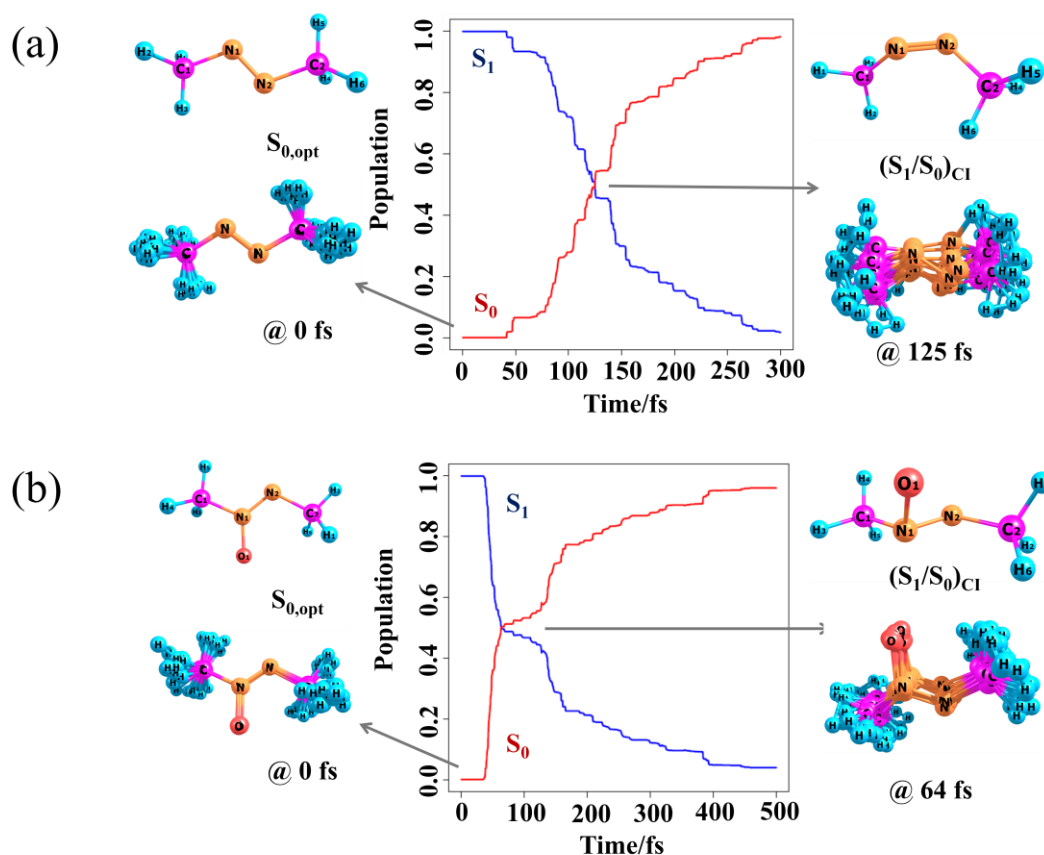


Figure 6: Plots of (a) average  $C1N1N2C2$  dihedral angle (in degree) of AM and (b) of average  $C1N1N2O1$  pyramidal angle (in degree) of AOM as a function of simulation time, as revealed by the AIMS simulation. Each data point in both figures represents an average of 28 and 36 independent AIMS simulations (with different initial conditions), respectively for AM and AOM. Error bar features the standard deviation of the mean value. Atom numbers are given in the respective molecular structure.

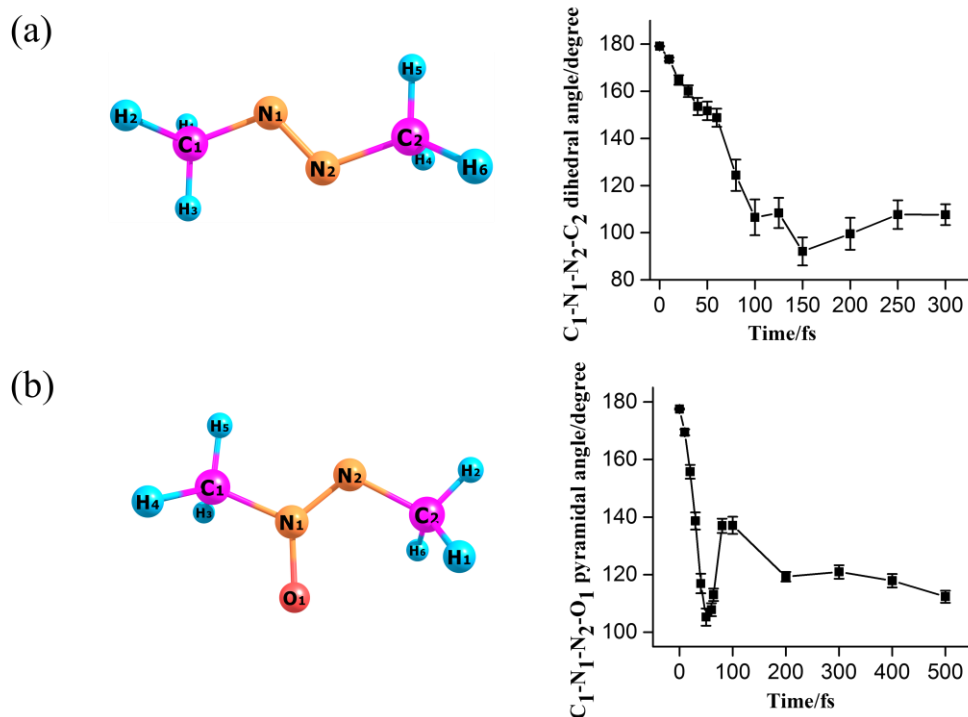


Figure 7: Plots of (a) average C-N bond distance (in Å) of AM and (b) of average C-N and N-O bond distances (in Å) of AOM as a function of the AIMS simulation time. Each data point in both figures represents an average of 28 and 36 independent AIMS simulations (with different initial conditions), respectively for AM and AOM.

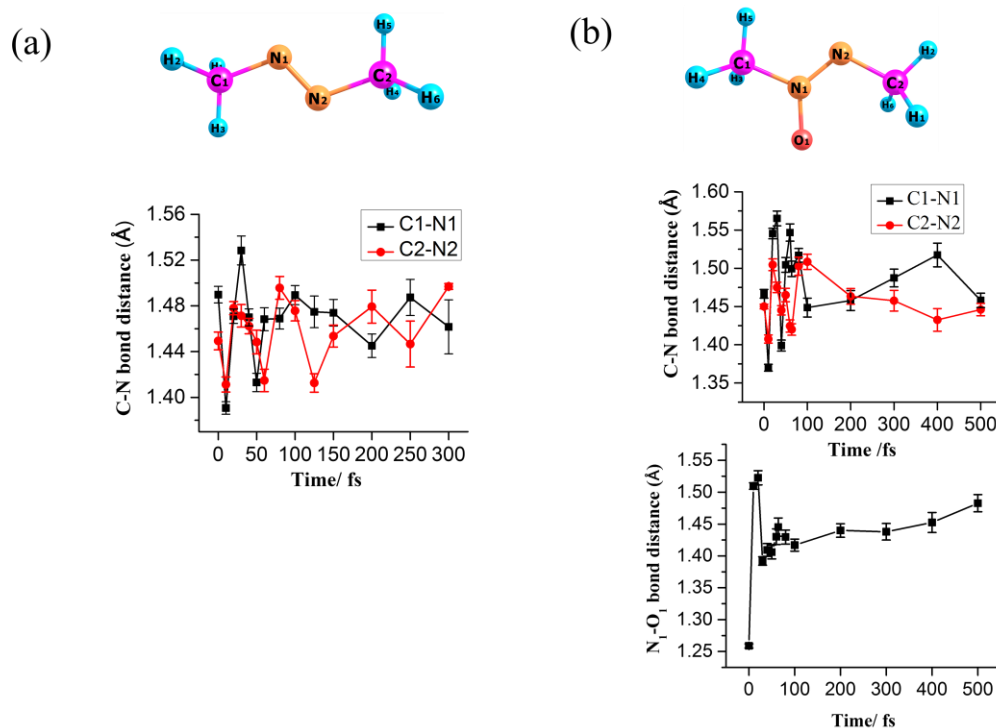




Figure 8: Plot of average population on the first excited state ( $S_1$ , blue) and on the ground state ( $S_0$ , red) of AM molecule as a function of simulation time (in femtosecond) along the (a) isomerization and (b) C-N bond dissociation pathways of AM, as revealed by AIMS simulation using state average-CASSCF(10,8)/6-31G(d) wave function. Sampled structures are also depicted to illustrate structural evolution of AM during the nonadiabatic relaxation process. (c) Plot of average C-N bond distance (in Å) of AM as a function of the AIMS simulation time for trajectories representing C-N bond dissociation. Total 60 independent AIMS simulations (with different initial conditions) were used.

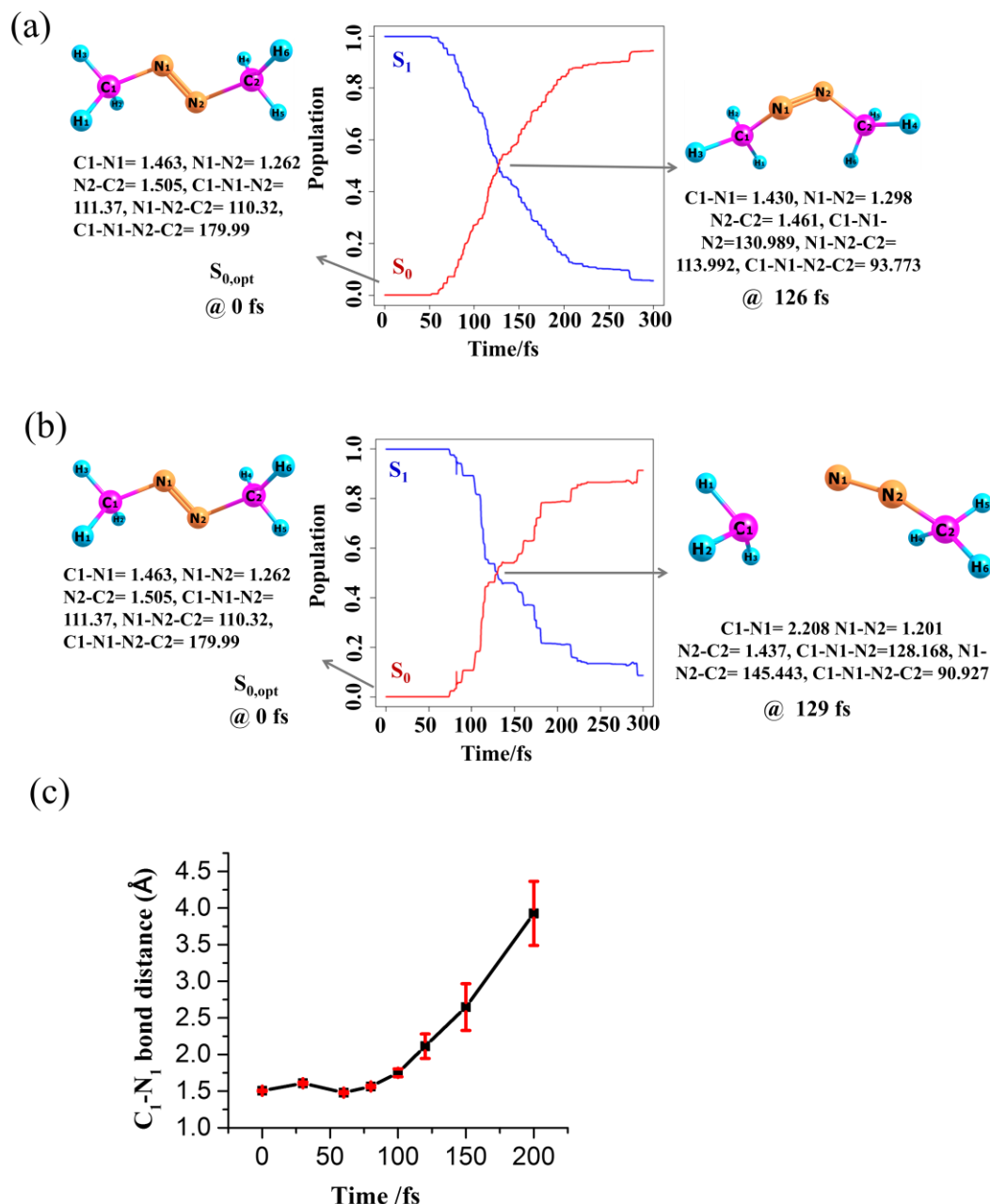


Figure 9: (a) Branching plane vectors of AM and AOM. (b) Energies of the ground state and the  $S_1(n,\pi^*)$  excited state near the  $(S_0/S_1)_{CI}$  conical intersection following displacements in the branching plane along the  $\vec{g}$  and  $\vec{h}$  vectors. These two vectors were calculated with the SA-CASSCF(6,4)/6-31G(d) wavefunction at the respective optimized MECI geometries which are shown in Figure 3.

